J Nanopart Res (2017) 19: 188
DOI 10.1007/s11051-017-3879-6

RESEARCH PAPER

Magnetic phases at the molecular scale: the case of cylindrical Co nanoparticles

Pablo Díaz · Eugenio E. Vogel · Francisco Munoz

Received: 26 January 2017 / Accepted: 2 May 2017 / Published online: 25 May 2017
© Springer Science+Business Media Dordrecht 2017

Abstract The magnetic phases of cobalt nanocylinders at the molecular scale have been studied by means of density functional theory together with micromagnetism. Diameters of the objects are under 1 nm. The magnetic phases resulting from first-principle calculations are far from obvious and quite different from both semiclassical results and extrapolations from what is measured for larger objects. These differences reinforce the importance of the quantum mechanical approach for small nanoscopic particles. One of the main results reported here is precisely the unexpected order in the last filled orbitals, which produce objects with alternating magnetic properties as the length of the cylinder increases. The resulting anisotropy is not obvious. The vortex phase is washed out due to the aspect ratio of the systems and the strength of the exchange constants for Co. Nevertheless, we do a pedagogical experiment by turning gradually down the exchange constants to investigate the kind of vortex states which are hidden underneath the ferromagnetic phases.

Keywords Nanoparticles · Nanowires · Magnetic phases · In-plane · Off-plane · Anisotropy · Biomedical applications

P. Díaz (✉) · E. E. Vogel
Departamento de Ciencias Físicas, Universidad de La Frontera, Casilla 54-D, Temuco, Chile
e-mail: pablo.diaz@ufrontera.cl

E. E. Vogel · F. Munoz
Centro para el Desarrollo de la Nanociencia y la Nanotecnología CEDENNA, Santiago 9170124, Chile

F. Munoz
Departamento de Física, Facultad de Ciencias, Universidad de Chile, Santiago, Chile

Introduction

Magnetic nanowires (Nielsch et al. 2005; Li et al. 2004; Bryan et al. 2012) and magnetic nanotubes (Vogel et al. 2010; Velázquez-Galván et al. 2014) have been studied for more than 15 years due to their unique properties. One of the lines of research is on their sizes since some applications could be enhanced at the smallest possible scale. One important line of application arises in medicine where magnetic nanoparticles are used in drug delivery and therapy which requires knowledge of their reacting properties in biological media (Raphael et al. 2010). At a more point-like medical application, very small particles are used as cell markers or cell tracers (Xie et al. 2008).

The magnetic behavior of magnetic nanostructures has been extensively studied (Antonel et al. 2015; Douvalis et al. 2016; Gómez-Polo et al. 2016), and from the theoretical side the use of the continuum

approximation (i.e., micromagnetism) is customary (Sayed et al. 2016). These models are focused and tested against nanostructures sized in the several nanometer range, according to the experimental data available. However, in the opposite limit, below 1 nm in some dimension, the situation is more subtle, the relevant interactions can be dramatically modified such that it is possible observed the quantum nature of the system. Therefore, the following question arises naturally: Are the magnetic phases already obtained for classical and semiclassical nanoscopic cylinders still valid for the quantum molecular cylinders? The question is pertinent since in the classical works a scaling law was proposed without any apparent limitation in size (D'Albuquerque e Castro et al. 2002; Landeros et al. 2006; Zhang et al. 2008). We propose to inquire whether the extrapolation of the classical results still holds for the dimensions of the quantum cylinders we investigate here, with the height H of the order of a few nanometer and diameter D just a decimal of a nanometer.

In the present paper, we study the magnetic phase diagram of subnanoscopic cylindrical clusters formed by a few dozen Co atoms. Such structures have proven to be stable for different cross sections (Aguilera-Granja et al. 2014; Aguilera-Granja, Faustino et al. 2016) from a theoretical point of view. We will use both, a quantum mechanical approach and also by treating a semiclassical way, considering the magnetic moments as independent of the orbital degrees of freedom. As we will see, the latter coincides with the results for classical nanoscopic cylinders (D'Albuquerque e Castro et al. 2002; Landeros et al. 2006; Zhang et al. 2008), in which three phases were reported: in-plane, out-of-plane, and vortex. In-plane refers to a ferromagnetic alignment with all spins parallel to the plane containing the atomic positions and perpendicular to the cylindrical axis. Out-of-plane refers to a ferromagnetic alignment with all spins parallel to the cylindrical axis and perpendicular to the plane. In the vortex states, all spins are on the plane perpendicular to the axis but slightly shifting orientations so their magnetization orientations close around in circles yielding nil total magnetization. These three phases are present in macroscopic systems. However, the vortex phase is not observed in the present systems, situation that will be analyzed. Our results show that although there exist some coincidences with the semiclassical approach, at this scale a full quantum mechanical approach is needed.

In the following section, we describe the methodology and the systems to be studied. In "Magnetic Hamiltonian: exchange and anisotropy constants," we present the magnetic Hamiltonian and its main consequences for the quantum particles. In "Results and discussion," we review the magnetic phases for tubes and wires. Section "Conclusions" is devoted to the main conclusions of this work. An Appendix devoted to nomenclature is included at the end of the paper.

Methodology and systems under study

The systems under study are cylinders at the subnanoscopic (or "molecular") level. There are five families of particles classified according to their cross sections. They correspond to those already reported by Aguilera-Granja et al. (2014) where they are individually illustrated. Here, we offer generic illustrations of the families in Fig. 1. In the Appendix, we present the nomenclature that we have used to label the nanoparticles.

The calculations were performed using the density functional theory as implemented within the Vienna ab initio simulation package (VASP) code (Kresse and Furthmüller 1996a, b; Kresse and Hafner 1993, 1994). Projected augmented-wave (PAW) (Blöchl 1994; Kresse and Joubert 1999) pseudopotentials were used with PBE as the exchange-correlation parametrization (Perdew et al. 1996, 1997). A large vacuum space (at least 15 Å) was considered. The energy cutoff of the plane waves was set to 350 eV. For all the structures considered here, we performed a ionic relaxation until the forces were negligible, $|\mathbf{F}| < 0.01$ eV/Å. A higher precision on the force limit or in other parameters does not produce any noticeable improvement on the total energies or anisotropies. We found a general agreement with the structures already proposed (see Fig. 1), despite using a different DFT implementation (Aguilera-Granja et al. 2014).

After a thorough energy minimization, the wave functions and charge densities were computed within the collinearity assumption and without spin-orbit coupling. These quantities were used as input for

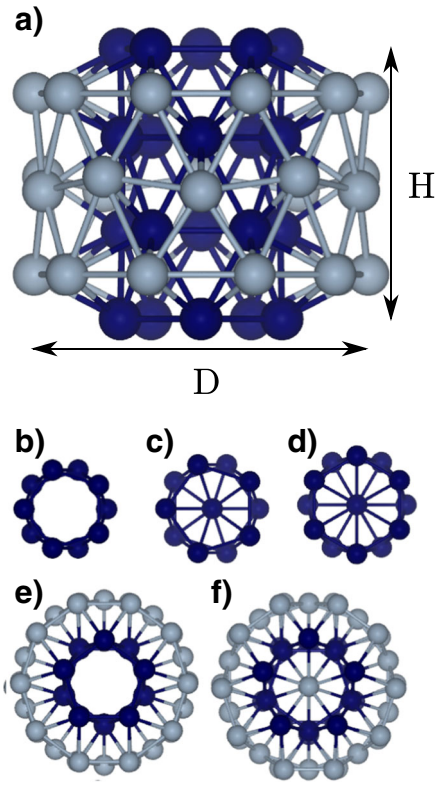

Fig. 1 Schematic views of the nanocylinders. **a** Lateral view of a nanotube composed by two kinds of concentric nanotubes: the *inner* (*outer*) nanotube is formed by 4(3) pentagonal (decagonal) rings of Co atoms; this system will be called T_{10}-50. **b** *Top* (or *bottom*) view of family T_5-N; **c** family W_5-N; **d** family $W_6 - N$; **e** family T_{10}-N; and **f** family $W_{10} - N$. *T* tube, *W* wire, *N* total number of atoms. The colors are just a help to the eye

the next step, which includes the spin-orbit term and allows the calculation of anisotropies by changing the quantization axis (Hobbs et al. 2000).

The found solutions allow us to calculate the exchange constants J which in general vary slightly for the different nearest-neighbor pairs of atoms through the particle. However, for simplicity, we shall assume that J is the same for all such pairs within each cylinder. This is a useful assumption to estimate the energy of the exchange interactions, which is orders of magnitude larger than the other energies involved (magnetocrystalline-like and shape anisotropies).

The calculations of magnetic properties were carried by a home-made micromagnetism program, using as a input the parameters taken from DFT together with a Heisenberg Hamiltonian and the Landau–Lifshitz–Gilbert equation (Landau and Lifshitz 1935; Gilbert 2004).

Magnetic Hamiltonian: exchange and anisotropy constants

In the absence of an external magnetic field, the contributions to the magnetic Hamiltonian are

$$\mathcal{H} = H_{\mathrm{H}} + H_{\mathrm{A}} + H_{\mathrm{Dip}}, \tag{1}$$

where the first term is the semiclassical Heisenberg Hamiltonian, H_{A} is the symmetry breaking term due to the positions of the atoms (it is equivalent to the magnetocrystalline anisotropy in solids), and H_{Dip} is the dipole-dipole interaction summing over all pairs of atoms in the system. In the remainder of this section, we will elaborate on each term of $\mathcal{H}$ calculating them for the different particles under study.

The Heisenberg Hamiltonian models the exchange energy:

$$H_{\mathrm{H}} = J \sum_{<i,j>} \hat{S}_i \cdot \hat{S}_j, \tag{2}$$

where the summation runs over the nearest neighbors with spins $\hat{S}_i$ and $\hat{S}_i$, respectively, for which J has been assumed constant within each system; the corresponding values of J obtained for the structures under consideration can be found in Table 1.

The second term in $\mathcal{H}$ (1) is the symmetry breaking term or magnetocrystalline anisotropy energy (H_{A}), arising from the spin-orbit coupling. Due to the cylindrical symmetry of the nanostructures here considered, the axial axis could be either the easy or the hard magnetic axis. This component of the Hamiltonian can be expressed as

$$H_{\mathrm{A}} = K \sum_i \sin^2(\theta_i), \tag{3}$$

where K is the anisotropy constant and θ_i is the angle formed by the i-th spin with the axial axis. A positive value of K means an axial easy axis, conversely, a negative value of K implies an easy plane perpendicular to the cylinder's axis. The values of K found here are listed in Table 1. The last term in the Magnetic

Table 1 Exchange constants, J, symmetry breaking (magnetocrystalline anisotropy) constants, K, and anisotropy constants from dipolar interactions, K_D

Rings	System	J	K	K_D
2	T_5-10	−44	0.56	−0.004
3	T_5-15	−46	0.09	0.012
4	T_5-20	−28	−0.03	0.019
5	T_5-25	−45	−0.03	0.027
6	T_5-30	−35	0.22	0.036
7	T_5-35	−44	0.84	0.038
2	W_5-11	−51	0.31	−0.013
3	W_5-17	−46	−0.06	0.003
4	W_5-23	−42	−0.07	0.011
5	W_5-29	−46	0.28	0.018
6	W_5-35	−50	0.21	0.026
7	W_5-41	−54	−0.17	0.026
2	W_6-13	−70	0.22	−0.012
3	W_6-20	−46	−0.17	0.001
4	W_6-27	−38	−0.27	0.013
5	W_6-34	−41	0.08	0.018
6	W_6-41	−44	−0.45	0.023
7	W_6-48	−39	0.24	0.026
3/2	T_{10}-35	−57	−0.06	−0.018
4/2	T_{10}-50	−56	−0.01	−0.004
5/4	T_{10}-65	−57	0.23	0.005
2/1	W_{10}-21	−57	−0.16	−0.038
3/2	W_{10}-37	−70	0.10	−0.019
4/2	W_{10}-53	−68	0.12	−0.006
5/4	W_{10}-69	−62	0.11	0.004

All values are given in meV. The "rings" field is the number of atomic rings composing the nanowire/nanotube; in the case of wider nanostructures, the inner and outer number of rings is given in the form inner/outer (see Fig. 1)

Hamiltonian comes from the dipole-dipole interactions. We assign a local magnetic moment at each site of the cluster, whose magnitude was obtained from the first-principle calculations, by integranting the spin-resolved charge density around each atom. The description was performed assuming that such magnetic moments correspond to ideal magnetic dipoles, described by a vector whose magnitude is preserved. Explicitly, the dipolar term in Eq. 1 is given by:

$$H_{\mathrm{Dip}} = \frac{\mu_0}{4\pi} \sum_{i,j} \frac{\mathbf{M}_i \cdot \mathbf{M}_j - 3\left(\mathbf{M}_i \cdot \hat{n}_{ij}\right)\left(\mathbf{M}_j \cdot \hat{n}_{ij}\right)}{r_{ij}^3}, \qquad (4)$$

where r_{ij} is the distance between atom pairs and $\mathbf{M}_i$ corresponds to magnetic moment of the atom i. To calculate the shape anisotropy arising from the dipolar interaction, we consider that the magnetic moments are completely aligned with each other due to previous components of the Hamiltonian and then we calculate the dipolar energy given by the Eq. 4 for two cases of alignment: direction on the axis and direction perpendicular to the axis (in-plane), E_{DA} and E_{DP}, respectively. Following an approach similar to the one described by Eq. 3, we define the dipolar anisotropy constant, K_D, as the energy difference between the two alignment cases: $K_D = E_{DP} - E_{DA}$. Accordingly, a positive value of K_D means an axial easy axis, conversely, a negative value of K_D implies an easy plane perpendicular to the axis. The values for the dipolar anisotropy constants per atom, K_D, are given in Table 1.

From a dynamic point of view, it is possible to find the ground state by solving the equation of Landau-Lifshitz-Gilbert (see Eq. 6), considering a random initial configuration; This technique is employed in "Vortex phase," where we show the changes in the individual magnetic moments. There, we will explore the behavior of the different nanocylinders obtained by (artificially) tuning the value of the exchange interactions from zero to their actual value.

Results and discussion

Magnetic phase diagrams

The main results of our calculations are summarized in Figs. 2 and 3; they show the diagrams of magnetic phases for wires and tubes, respectively. These nanostructures are sorted in function of their length (H) and diameter (D), considering the data of Table 1. To avoid ambiguity the external dimensions D and H are measured considering point-like atoms. The blue (red) symbols represent easy (hard) axis systems respectively. Figures 2a and 3a show the results obtained from the full magnetic Hamiltonian (1), while Figs. 2b and 3b ignore the symmetry breaking term H_{A} (see Eq. 3), but include the anisotropy arising from dipolar interactions. We define the dimensions of the nanocylinders according to their atomic positions after the a structural optimization.

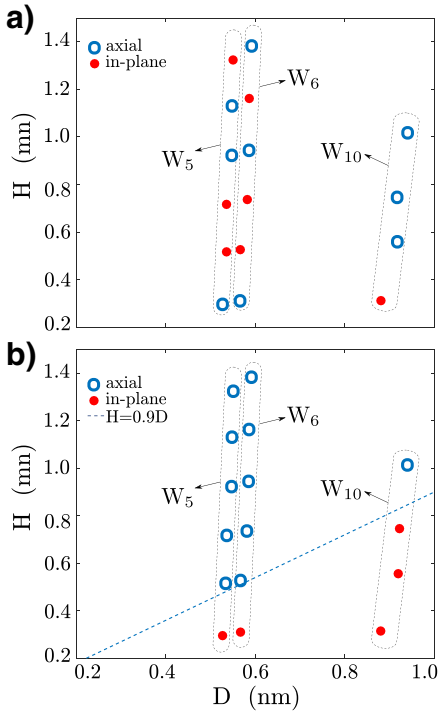

Fig. 2 Magnetic phase diagram for the easy axis orientations of the nanowires studied here. The *upper panel* indicates the actual orientations of the magnetization according to the full Hamiltonian given by Eq. 1. The *lower panel* shows the magnetization orientations obtained by the semiclassical Hamiltonian of Eq. 5. The *dotted line* corresponds to the extrapolation for wires from the continuum model (see the main text). Boxes are included to help the eye to identify families

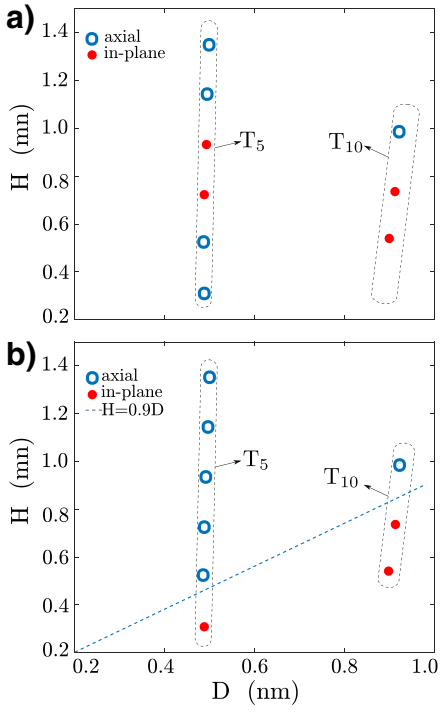

Fig. 3 Magnetic phase diagram of the easy axis orientation of the nanotubes. The *upper panel* indicates the actual orientation of the magnetization according to the full Hamiltonian given by Eq. 1. The *lower panel* shows the magnetization orientations obtained by the semiclassical Hamiltonian of Eq 5. The *dotted line* corresponds to the extrapolation for wires from the continuum model (see the main text). Boxes are included to help the eye to identify families

The dotted line corresponds to $H = 0.9D$ obtained for classical systems sized in tens of nm (D'Albuquerque e Castro et al. 2002). It can be noticed that this line agrees well with the semiclassical approach that ignores the spin-orbit interaction. However, this extrapolation certainly disagrees with the quantum calculations.

By observing the case employing the full Hamiltonian (Figs. 2a and 3a), it is evident that the behavior for systems on the scale of tens of nanometers disagrees from the semiclassical approach when applied to the scale of few atoms, where the quantum phenomena play an important role, for both wires and tubes. However, if we ignore the quantum effects arising from the spin-orbit coupling, we observe a total agreement with the aforementioned continuum model, even tough that model was developed for much longer nanocylinders treated by means of micromagnetic computational techniques.

Quantum features

The most striking feature that pops up from running over the fourth column of Table 1 is that not one trend is to be found in the symmetry breaking anisotropy, K. This is a clear manifestation of quantum effects for these small systems that present discrete energy level schemes of varying magnetic properties as it is shown in Fig. 4 and discussed below. This progressive filling of discrete energy levels produces strong oscillations of the resulting magnetic moments of the systems (Munoz et al. 2013; Dorantes-Davila and Pastor 2005; Gambardella et al. 2002; Hong and Wu 2003) which resembles molecular magnetism.

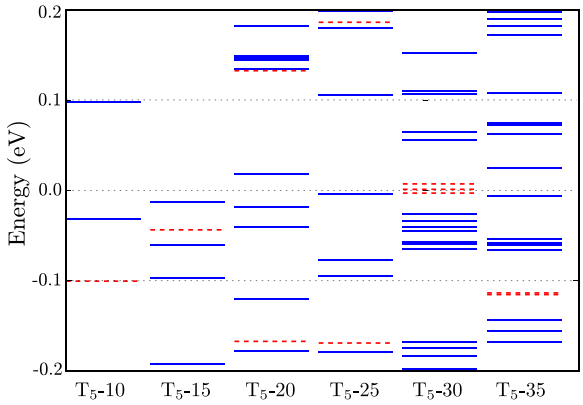

Fig. 4 Electronic levels for T_5-N nanocylinders close to the Fermi energy. *Continuous* or *dashed lines* (reinforced by different colors) denote different spin states

While it is well-known that the source of H_A comes from the spin-orbit interaction, theoretically, this is a very complex subject to deal with. Up to the best of our knowledge the only models of H_A in the literature consider systems larger than ours with a dominant symmetry which are not applicable here. Therefore, instead of providing any theoretically insight of the actual values found in Table 1, we will present arguments that support the lack of patterns in the found result.

Let us begin by illustrating this point by means of a much simpler system: an infinite mono-atomic wire. The symmetry of the wire (crystal field) implies a splitting of d orbitals depending on their orientations. This defines the angular momentum. Since spin-orbit coupling, $\mathbf{L} \cdot \mathbf{S}$, is much weaker than the crystal field, it is reasonable to think that $\mathbf{L}$ is fixed independently of $\mathbf{S}$. Then, the only role of the spin-orbit coupling would be to align $\mathbf{S}$ parallel to the direction of $\mathbf{L}$, which in turn depends on characteristics of the mono-atomic wire. Then, the length, width, and shape become important parameters to determine the way the energy levels are filled up.

As we turn now our attention to the particles under study, we notice that the simplest clusters are those belonging to the series T_5, where any atom has two different types of neighbors: those from the same ring and the ones belonging to adjacent rings. This difference effectively splits the d orbitals according to their orientations, but in practice the linear combinations of atomic orbitals, building an eigenstate are very similar, partially because the nearest-neighbor distances are similar for both orientations of neighbors. As the sizes of the systems increase, the positions of the atoms on the rings along the axis make a difference both in the number of nearest neighbors and the nearest-neighbor distances. This means complicated energy level schemes changing abruptly for one cluster to next one in the family as N grows. This effect leads to variable properties in the last occupied electronic levels, effectively making every cluster different from the others. In particular, the magnetic property of each cylinder is quantum mechanically decided not following any classical trend. This is illustrated in Fig. 4 where the energy levels corresponding to different spin (continuous and dashed lines) can be found at different, unrelated, energy positions as we go along the family of tubes. Also there is no trend in the orbital character of those energy levels (not shown). Thus, the Fermi energy position (or equivalent for these molecular objects) determines the magnetic character of each particle without following any trend. Diagrams similar to Fig. 4 can be constructed for the other families all showing a non trivial ordering of energy levels.

Conversely, even thought the value of J varies from system to system, for most of them $J \sim 50$ meV indicating a strong ferromagnetic behavior regardless of the exact nature of the system. Therefore, we safely can use this parameter in continuum approximation, at least is strongly ferromagnetic systems such as Co.

Our results indicate that the dipolar interaction—compared to the other magnetic interactions—does not play any significant role at this scale, in strong contrast to the behavior found for longer systems (D'Albuquerque e Castro et al. 2002). We found that, for most cases, the magnitude of K_D is much smaller than both, J and K, showing that the anisotropy resulting from the dipolar interaction is not relevant at this level.

Vortex phase

As it can be appreciated from previous discussion the vortex phase—a ubiquitous phase of magnetic nanocylinders—is missing in the tubes and wires considered in this study. Once the spins are in the plane, they minimize their energy by adopting a parallel alignment. Since there is a small number of atoms in each ring, the angle between consecutive spins in a vortex would imply a significant energy cost, (see Eq. 2), for instance, for T_6 this angle is $\pi/3$, larger

than the parallel alignment in the ferromagnetic case. A strong enough dipolar interaction could overcome the exchange term, leading to a vortex state in these rings, but, conversely, in our small systems, this interaction is extremely weak. In microscopical cylindrical systems, two factors favor the vortex state: on one hand, the rings are larger and they can be though of as formed by a great number of atoms with only a slight deviation in the magnetization between consecutive atoms; on the other hand, the long-range dipolar field adds up a huge number of interactions to the point it can compete with the exchange interactions in some cases.

In spite of the fact our systems do not present the vortex phase, we can use them to test the conditions under which a vortex phase could appear. To accomplish this task, we can vary the parameters of the Hamiltonian, searching for the possibility of vortex configurations that could be energetically competitive with the other already established phases. One such possibility is to tune the magnitude of the exchange interaction J and to ignore the anisotropy coming from the spin-orbit coupling ($K = 0$). Starting from the localized magnetic moments obtained from the first-principle calculations, the magnetic dipoles can interact according to the normalized semiclassical Hamiltonian:

$$H_{SC} = -J_n \sum_{\langle i,j \rangle} \mathbf{m}_i \cdot \mathbf{m}_j + \sum_{i<j} \frac{\mathbf{m}_i \cdot \mathbf{m}_j - 3(\mathbf{m}_i \cdot \hat{n}_{ij})(\mathbf{m}_j \cdot \hat{n}_{ij})}{d_{ij}^3}, \quad (5)$$

where the first summation runs over first neighbors and the second summation runs over all pairs of atoms. The normalized constant exchange interaction is given

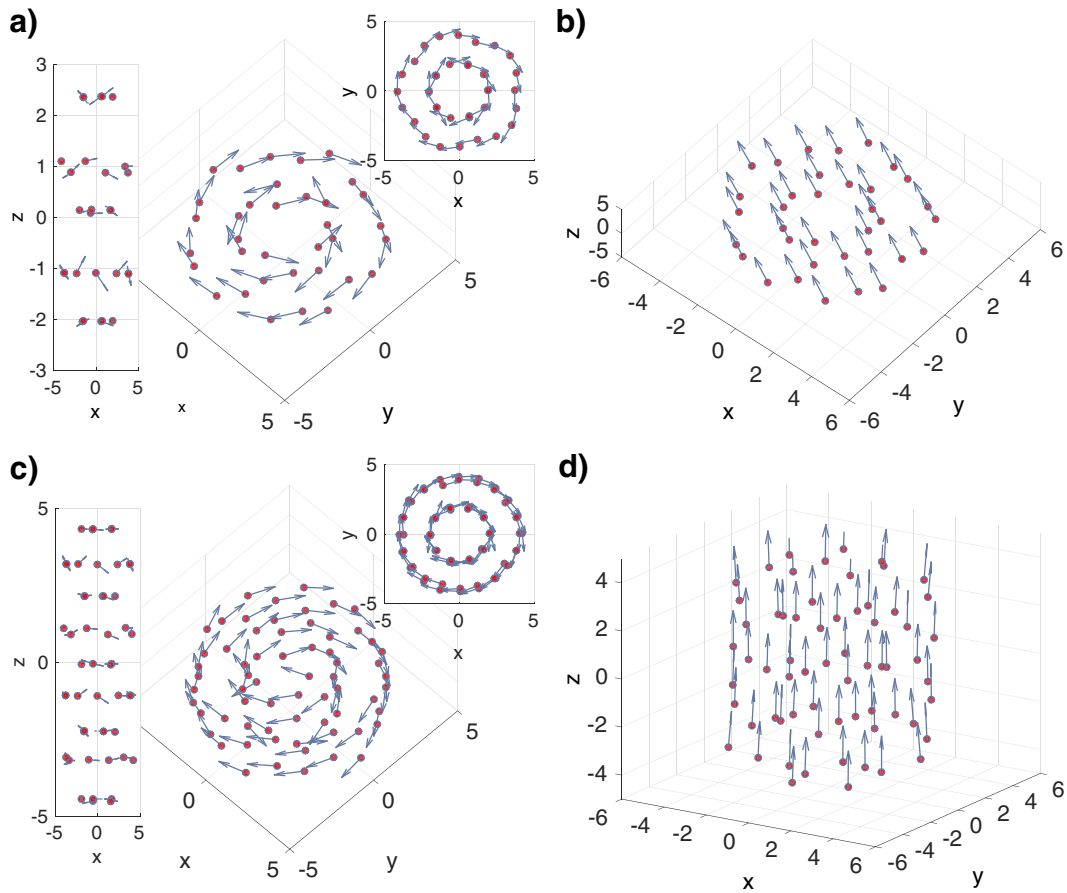

Fig. 5 Magnetic configurations for the semiclassical approach. **a** T_{10}-35 lateral, diagonal and top views for $J_n = 0$. **b** Same system under diagonal view for $J_n = 0.5$. **c** T_{10}-65 lateral, diagonal and top views for $J_n = 0$. **d** Same system under diagonal view for $J_n = 0.5$

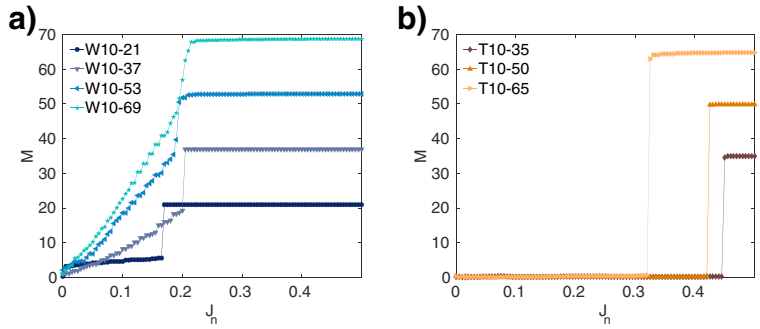

Fig. 6 Transition from a vortex configurations to ferromagnetic configurations for **a** wires W_{10} and **b** tubes T_{10} as the exchange constant is increased

by $J_n = -18.6\ J/M_s^2$ with J in meV and M_s is the average value of the magnetic moment per atom in units of μ_B (for T_{10}-35 case $J = -57$ meV and $M_s = 1.97$, such that $J_n = 273.2$). The distance between atom pairs, d_{ij}, is given in Å and $\mathbf{m}_i = \mathbf{M}_i/M_s$ corresponds to magnetic moment of the atom i in units of M_s. In this frame, the magnetic configuration is given by the orientation of each individual magnetic moment $\mathbf{m}_i$.

From a deterministic point of view, temporal evolution of each $\mathbf{m}_i$ is ruled by Landau-Libshitz-Gilbert equation (Landau and Lifshitz 1935; Gilbert 2004):

$$\frac{d\mathbf{m}^i}{dt} = -\mathbf{m}^i \times \mathbf{h}^i_{eff} + \alpha \mathbf{m}^i \times \frac{d\mathbf{m}^i}{dt}, \tag{6}$$

where time is measured in $(|\gamma|M_s)^{-1}$ units, with γ the gyromagnetic constant. The Gilbert parameter α in Eq. 6 introduces the interaction of each particle with the external environment. Although particles can gain or lose energy, we consider dissipative environments ($\alpha > 0$). Further, $\mathbf{h}^i_{eff} = -\nabla^i H_{SC}$ is the effective field acting over particle i. Thus, a system of magnetic particles with a random initial configuration at $t = 0$ will evolve until it reaches a stationary configuration at $t = \tau_R$ (relaxation time). To solve this system of coupled differential equations, we have applied the Fourth Order Runge Kutta (RK4) integration method.

The magnetic configurations found in T_{10}-35 and T_{10}-65, for $J_n = 0$ are presented in the Fig. 5a, c, respectively. In both cases, a vortex configuration is obtained. Increasing J_n to a value of 0.5 (its actual value is 273.2) shows that the magnetic configuration changes to a ferromagnetic state, which is in-plane for T_{10}-35 (Fig. 5b) and parallel to the axial axis for T_{10}-65 (Fig. 5d). The previous results confirm again that the ferromagnetic phases are absolutely dominant for these systems. Furthermore, it is observed that for T_{10}-35 the ferromagnetic lower energy state is reached in the plane, whereas for T_{10}-65 is on the axis, consistent result with both semiclassic and first-principle calculations as it can be seen in Fig. 3.

This transition between the two states—vortex and ferromagnetic—can be appreciated by the magnetization as it can be seen in Fig. 6. Here, J_n is gradually increased in the range [0.0–0.5] for all the decagonal systems, with Fig. 6a for wires and Fig. 6b for tubes. It can be noticed that the vortex to ferromagnetic transition is abrupt for tubes while it is gradual for wires. Thus, the highly connected atoms on the wire axis soften the transition.

Conclusions

The leading magnetic energy is the exchange term, indicating ferromagnetic states for all the cylinders studied here.

In general terms, we can speak of systems with exchange interactions around −40 meV, anisotropy fields of the order of 0.2 meV reaching down to about −0.1 meV, and dipolar contributions of the order of 0.01 to −0.01 meV. Modulations are appreciated in Table 1.

However, the magnetic orientation (in-plane or off-plane) of each system is a consequence of ordering of its energy levels and the ways they fill up with the available electrons. This means abrupt changes of magnetic properties as the cylinders add more rings to reach longer lengths within each family.

At this scale, the magnetic phases are not obvious and full quantum mechanics (including spin-orbit interactions) is necessary to fully describe these systems. This means that the classical or semiclassical description of these cylinders fails at a point which

makes impossible to extrapolate the phases found at the nanoscopic or larger systems. In particular, the preference for in-plane or out-of-plane phases is completely determined by the quantum mechanical properties.

The vortex state is lost at this scale since it is energy costly to close the interactions within the plane for a low number of magnetic moments. However, we can attempt to visualize the way the dipolar interaction could manifest itself in very large systems by tuning down the exchange interactions. When this is done, we are able to recover the vortex state which emerges mainly for the tubes and shorter cylinders as it might be expected classically. When the exchange constant is let to gradually increase from zero value the ferromagnetic phase is recovered abruptly for tubes and gradually for wires.

The main message is that these particles present interesting properties which can be modulated by their geometries. However, each one has to be characterized separately from the rest since quantum mechanics inhibit extrapolations or family trends, and therefore, the continuum approximation, unless a weak anisotropy is to be expected.

Finally, for the future work, while in the present study, we showed the dominance of the quantum effects at molecular scale, it would be helpful to estimate at which size a classical description start to be valid. Answering this issue is overwhelming difficult, but instead, a simple model could provide some information of the length scales.

Compliance with Ethical Standards

Conflict of interest The authors declare that they have no conflict of interest.

Funding This work was partially supported by the Universidad de La Frontera DIUFRO project under grant DI14-0067. Partial support from the following Chilean sources is acknowledged: Fondecyt (Chile) under contracts 1150019, 1150806 and Financiamiento Basal para Centros Científicos y Tecnológicos de Excelencia (Chile) through the Center for Development of Nanoscience and Nanotechnology (CEDENNA, Contract FB0807).

Appendix: Nomenclature

Pentagonal tubes The basic unit is a pentagonal ring of Co atoms. The tube grows by adding these pentagons in an intercalated way thus minimizing energy. A projection of the atoms on any end of the cylinder is presented in Fig. 1b. They are denoted by T_5-N, where N is the total number of atoms in the particle: $N = 5 \times R$, with R representing the number of rings conforming the tube. We will consider from T_5-10 to T_5-35.

Pentagonal wires The basic units are a pentagonal ring of Co atoms and a single Co atom over the center of such pentagon. The wires grow intercalating the axial atom in between consecutive rings; a projection of the atoms on any end of the cylinder is presented in Fig. 1c. These wires are denoted by W_5-N, where N is the total number of atoms in the particle: $N = 5 \times R + (R-1)$, with R representing the number of rings conforming the wire. At the ends of the cylinder only pentagons are allowed. We will consider from W_5-11 to W_5-41.

Hexagonal wires The basic units are hexagonal rings of Co atoms and a single Co atom over the center of such hexagon. The wires grow intercalating the axial atom in between consecutive rings; a projection of the atoms on any end of the cylinder is presented in Fig. 1d. These wires are denoted by W_6-N, where N is the total number of atoms in the particle: $N = 6 \times R + (R-1)$, with R representing the number of rings conforming the wire. At the ends of the cylinders only hexagons are allowed. We will consider from W_6-13 to W_6-48.

Decagonal tubes The basic units are a pentagonal rings and decagonal rings of Co atoms. These tubes are grown alternating pentagons and decagons along the cylindrical axis; a projection of the atoms on any end of the cylinder is presented in Fig. 1e. These tubes are denoted by T_{10}-N, where N is the total number of atoms in the particle: $N = 5 \times R + 10 \times (R-1)$, with R representing the number of pentagons conforming the tube. We will consider from T_{10}-35 to T_{10}-65. Figure 1a shows a lateral view of T_{10}-50.

Decagonal wires The basic units are single axial atoms, pentagonal rings and decagonal rings of Co atoms. These tubes are grown similarly to the decagonal tubes but in addition they also have a single atom on the axis at approximately the same height as the external decagon; a projection of the atoms on any end

of the cylinder is presented in Fig. 1f. These wires are denoted by W_{10}-N, where N is the total number of atoms in the particle: $N = 5 \times R + 10 \times (R-1) + (R-1)$, with R representing the number of pentagons conforming the tube. We will consider from W_{10}-21 to W_{10}-69.

We should mention that the family of hexagonal tubes (T_6-N) is not included here because we failed to find stable structures for this theoretical conception. When initiations with this symmetry were started from several possible configurations they all collapsed into non cylindrical particles.

References

Aguilera-Granja F, Montejano-Carrizales JM, Vogel EE (2014) Structural and electronic properties of magnetic cylinders at the atomic scale. Eur Phys J D 68(2):38

Aguilera-Granja F, Montejano-Carrizales JM, Vogel EE (2016) Structural and oxidation properties of coni nanowires. Eur Phys J D 70(6):137

Antonel PS, Oliveira CLP, Jorge GA, Perez OE, Leyva AG, Negri RM (2015) Synthesis and characterization of cofe2o4 magnetic nanotubes, nanorods and nanowires. formation of magnetic structured elastomers by magnetic field-induced alignment of cofe2o4 nanorods. J Nanoparticle Res 17(7):294

Blöchl PE (1994) Projector augmented-wave method. Phys Rev B 50:17953–17979

Bryan MT, Bance S, Dean J, Schrefl T, Allwood DA (2012) Transverse and vortex domain wall structure in magnetic nanowires with uniaxial in-plane anisotropy. J Phys Condens Matter 24(2):024205

D'Albuquerque e Castro J, Altbir D, Retamal JC, Vargas P (2002) Scaling approach to the magnetic phase diagram of nanosized systems. Phys Rev Lett 88:237202

Dorantes-Davila J, Pastor GM (2005) Magnetic reorientation transitions along the crossover from one-dimensional to two-dimensional transition-metal nanostructures. Phys Rev B 72:085427

Douvalis AP, Bourlinos AB, Tucek J, Čépe K, Bakas T, Zboril R (2016) Development of novel fept/nanodiamond hybrid nanostructures: L10 phase size-growth suppression and magnetic properties. J Nanoparticle Res 18(5):115

Gambardella P, Dallmeyer A, Maiti K, Malagoli M, Eberhardt W, Kern K, Carbone C (2002) Ferromagnetism in one-dimensional monatomic metal chains. Nature 416(6878):301–304

Gilbert TL (2004) A phenomenological theory of damping in ferromagnetic materials. IEEE Trans Magn 40(6):3443–3449

Gómez-Polo C, Larumbe S, Barquín LF, Fernández LR (2016) Magnetic induction heating as a new tool for the synthesis of fe3o4–tio2 nanoparticle systems. J Nanoparticle Res 18(5):118

Hobbs D, Kresse G, Hafner J (2000) Fully unconstrained non-collinear magnetism within the projector augmented-wave method. Phys Rev B 62(17):11556–11570

Hong J, Wu RQ (2003) First principles calculations of magnetic anisotropy energy of co monatomic wires. Phys Rev B 67:020406

Kresse G, Furthmüller J (1996a) Efficiency of ab-initio total energy calculations for metals and semiconductors using a plane-wave basis set. Comput Mat Sci 6:15

Kresse G, Furthmüller J (1996b) Efficient iterative schemes for ab initio total-energy calculations using a plane-wave basis set. Phys Rev B 54:11169–11186

Kresse G, Hafner J (1993) Ab initio molecular dynamics for liquid metals. Phys Rev B 47:558–561

Kresse G, Hafner J (1994) Ab initio molecular-dynamics simulation of the liquid-metal amorphous-semiconductor transition in germanium. Phys Rev B 49:14251–14269

Kresse G, Joubert D (1999) From ultrasoft pseudopotentials to the projector augmented-wave method. Phys Rev B 59:1758–1775

Landau LP, Lifshitz EM (1935) On the theory of the dispersion of magnetic permeability in ferromagnetic bodies. Phys Z Sowjetunion 8:153–169

Landeros P, Escrig J, Altbir D, Bahiana M, e Castro J (2006) Stability of magnetic configurations in nanorings. J Appl Phys 100(4):044311

Li F, Wang T, Ren L, Sun J (2004) Structure and magnetic properties of co nanowires in self-assembled arrays. J Phys Condens Matter 16(45):8053

Munoz F, Romero AH, Mejia-Lopez J, Moran-Lopez JL (2013) Finite size effects on the magnetocrystalline anisotropy energy in fe magnetic nanowires from first principles. J Nanopart Res 15(4):1–11

Nielsch K, Castano FJ, Matthias S, Lee W, Ross CA (2005) Synthesis of cobalt/polymer multilayer nanotubes. Adv Eng Mater 7(4):217–221

Perdew JP, Burke K, Ernzerhof M (1996) Generalized gradient approximation made simple. Phys Rev Lett 77:3865–3868

Perdew JP, Burke K, Ernzerhof M (1997) Generalized gradient approximation made simple [phys. rev. lett. 77, 3865 (1996)]. Phys Rev Lett 78:1396–1396

Raphael MP, Christodoulides JA, Qadri SN, Simpkins BS, Byers JM (2010) Magnetic moment degradation of nanowires in biological media: real-time monitoring with squid magnetometry. Nanotechnology 21(28):285101

Sayed F, Labaye Y, Sayed Hassan R, El Haj Hassan F, Yaacoub N, Greneche J-M (2016) Size and thickness effect on magnetic structures of maghemite hollow magnetic nanoparticles. J Nanoparticle Res 18(9):1–11

Velázquez-Galván Y, Martínez-Huerta JM, Medina JDLT, Danlée Y, Piraux L, Encinas A (2014) Dipolar interaction in arrays of magnetic. J Phys Condens Matter 26(2):026001

Vogel EE, Vargas P, Altbir D, Escrig J (2010) Handbook of nanophysics, vol 4. CRC press,

Xie J, Chen L, Varadan VK, Yancey J, Srivatsan M (2008) The effects of functional magnetic nanotubes with incorporated nerve growth factor in neuronal differentiation of pc12 cells. Nanotechnology 19(10):105101

Zhang W, Singh R, Bray-Ali N, Haas S (2008) Scaling analysis and application: Phase diagram of magnetic nanorings and elliptical nanoparticles. Phys Rev B 77:144428